Morphology of Poly(styrene-co-butadiene) Random Copolymer Thin Films and Nanostructures on a Graphite Surface

The Morphology of Poly(styrene-co-butadiene) Random Copolymer Thin Films and Nanostructures on a Graphite Surface

Jake McClements,[a] Michael P. Shaver,[b] Khellil Sefiane,[a] and Vasileios Koutsos [,a]*

[a] School of Engineering, Institute for Materials and Processes, The University of Edinburgh, Sanderson Building, King's Buildings, Edinburgh EH9 3FB, United Kingdom

[b]EaStCHEM School of Chemistry, University of Edinburgh, Joseph Black Building, King's Buildings, David Brewster Road, Edinburgh EH9 3FJ, United Kingdom

Abstract

We studied the morphology of poly(styrene-co-butadiene) random copolymers on a graphite surface. Polymer solutions were spin coated onto graphite, at various concentrations and molecular weights. The polymer films and nanostructures were imaged using atomic force microscopy. Above the overlap concentration, thin films formed. However, total wetting did not occur, despite the polymers being well above their T_g. Instead, dewetting was observed suggesting the films were in a state of metastable equilibrium. At lower concentrations, the polymers formed networks, nanoislands, and nanoribbons. Ordered nanopatterns were observed on the surface; the polymers orientated themselves due to π-π stacking interactions

reflecting the crystalline structure of the graphite. At the lowest concentration, this ordering was very pronounced. At higher concentrations, it was less defined but still statistically significant. Higher degrees of ordering were observed with poly(styrene-co-butadiene) than polystyrene and polybutadiene homopolymers as the copolymer's aromatic rings are distributed along a flexible chain which maximises π-π stacking. At the two lowest concentrations, the size of the nanoislands and nanoribbons remained similar with varying molecular weight. However, at higher concentrations, the polymer network features were largest at the lowest molecular weight indicating that in this case, a large proportion of shorter chains stay on top of the adsorbed ones. The contact angles of the polymer nanostructures remained mostly constant with size, which is due to the strong polymer/graphite adhesion dominating over line tension and entropic effects.

Introduction

Controlling and understanding the behaviour of polymers on surfaces is important for the successful development of many applications including surface nanopatterning,[1] functional membranes,[2] and composite materials.[3] Polymers are often used as a component in high performance composite materials due to their high toughness and low manufacturing cost.[4] This has led to polymer based composites frequently replacing traditional materials in many applications, such as components for cars and aircrafts.[5,6] The interface between the polymer matrix and filler components in composite materials is extremely influential in determining the materials bulk physicochemical properties.[7] Despite this, the interactions between polymers and filler materials are often poorly understood at a fundamental level. Studies have shown that polymer behaviour can be different at an interface in comparison to behaviour in the bulk.[8–11] However, the underlying physicochemical origins for the deviations in behaviour are often unknown or simply unexplored. If the behaviour of polymers at surfaces were more

thoroughly understood at a fundamental level, then this would aid in both the design and manufacture of polymer coatings, thin films, and composite materials with enhanced properties.

Composite materials that utilise the polymer/carbon interface have been used in numerous applications for many years.[12] Carbon black particles are used to reinforce elastomeric rubbers in the manufacture of car tyres, which significantly increases properties such as the tensile strength, stiffness, and abrasion resistance of the tyres.[13] Carbon fibres are woven together and embedded into epoxy resins to create a lightweight composite material with very high strength properties which can be used for many structural applications.[14,15] In more recent years, the discovery of carbon 'super materials' such as carbon nanotubes (CNTs) and graphene have led to further advancements in polymer/carbon nanocomposites.[3,16–19] The understanding of the carbon/polymer interface is vital for improving the physicochemical properties of composite materials. However, there are still many open questions regarding the fundamental behaviour of polymers at carbon surfaces.[20,21]

Studying the polymer/carbon interface is an area of extensive research. This research commonly includes investigating the electrical properties of carbon/polymer composites,[22,23] studying the interactions between carbon nanotubes and polymers,[24,25] and studying the self-assembly of polymers on graphene for nanolithography applications.[26–29] Atomic force microscopy (AFM) can also be used as an imaging technique to study the behaviour of many different organic molecules including polymers, on graphite surfaces at the nanoscale.[30,31] Many AFM studies have focused on characterising the distinct ordering of polymers on graphite. This behaviour is commonly observed in crystalline polymers, such as polyethylene. In these instances, the dimensions of the c-axis of the polyethylene crystal cell are very

similar to the graphite lattice constant. This encourages epitaxial interactions, which create a distinctly ordered polymer morphology.[32] A similar effect is also reported for polymers with alkyl chains. The distance of the 1,3-methylene group in trans alkyl chains is very similar to the graphite lattice constant, which also creates an ordered polymer morphology.[33–35] Investigations into the distinct ordering of amorphous linear polymers on graphite is a mostly unexplored area, and this could prove useful for nanopatterning applications. To our knowledge, there are no studies which comprehensively characterise polymer thin films, networks, nanoislands and nanoribbons on graphite, across a wide range of concentrations and molecular weights. Furthermore, investigations into the behaviour of linear amorphous copolymers, such as poly(styrene-co-butadiene) on graphite are limited. As far as we are aware, there are no studies investigating the specific ordering of poly(styrene-co-butadiene) on graphite. This is surprising as these polymers are extensively utilised within industry for polymer/carbon composite applications and would serve as a model system of graphitised carbon black.

This study investigates the morphology of poly(styrene-co-butadiene) random copolymer nanostructures on a graphite surface. The relationship between polymer morphology and solution concentration is thoroughly explored. This includes a detailed analysis of the ordering of the polymer nanostructures on graphite. Additionally, an investigation into how varying molecular weight impacts polymer morphology is presented. Finally, we include a study examining the contact angles of the polymer nanostructures.

Experimental Section

Previously, we investigated the formation of poly(styrene-co-butadiene) random copolymers on a mica surface.[36] The preparation of polymer samples and AFM methodology are the same in both studies, but the mica substrates are replaced with graphite.

Materials

Three samples of poly(styrene-co-butadiene) random copolymers were provided by Michelin. Their molecular weights (M_n) were 46 kg/mol, 86 kg/mol, and 355 kg/mol. The samples had styrene-butadiene ratios of 25.9:74.1, 26.3:73.7, and 25.9:74.1, and were monodisperse with Đs of 1.03, 1.01, and 1.02 for the 46 kg/mol, 86 kg/mol, and 355 kg/mol samples, respectively. Michelin conducted differential scanning calorimetry (DSC) on the samples which gave similar glass transition temperatures (T_g) of -36.4˚C, -35.1˚C, and -35.4˚C for the 46 kg/mol, 86 kg/mol, and 355 kg/mol samples, respectively. ZYA highly ordered pyrolytic graphite (HOPG) substrates were purchased from Scanwel Ltd. The molecular weights of the poly(styrene-co-butadiene) samples were significantly larger than the entanglement molecular weights of polystyrene (~13.5 kg/mol) and polybutadiene (~1.9 kg/mol).[37,38] This means that polymer samples in the study were able to entangle with one another.

Sample Preparation

The poly(styrene-co-butadiene) samples were prepared in toluene solutions. The solutions were made according to the polymer's overlap concentrations, c^*. This is the concentration in which polymer chains in solution will begin to overlap with one another.[39] The overlap concentrations were calculated theoretically for each sample using the following equation:[40]

$$c^* = \frac{M_n}{V_p N_A} \quad (1)$$

Where M_n is molecular weight, V_p is the pervaded volume, and N_A is Avogadro's number. The solutions were prepared at 3c*, 1c*, 0.1c*, 0.01c*, and 0.001c*. A table can be found in the ESI, which provides the corresponding concentrations by weight. In addition, the concentration by weight values are provided in the captions of Figures 1 – 3. The graphite surfaces were cleaved with scotch tape immediately before solution deposition. Spin coating was then carried out at 4000 rpm for 90 seconds in all experiments. The samples were then dried with nitrogen before being left overnight in a fume hood (16 – 72 hours).

Atomic Force Microscopy (AFM)

AFM was used to image the polymer formation on the graphite surface at the nanoscale. A Bruker Multimode/Nanoscope IIIa (Bruker, Santa Barbara, Ca, USA) was used for all imaging. To improve image resolution, two scanners were used: a J-scanner and an E-scanner with x-y ranges of ~160 μm and ~15 μm, respectively. All experiments were carried out using tapping mode in air at ambient conditions. For all experiments, Bruker RTESPA cantilevers were used with a nominal resonant frequency of 300 kHz, a nominal spring constant of 40 N/m, and a nominal tip radius of 8 nm. The freeware Gwyddion (http://gwyddion.net/) was used for all image processing and analysis.[41]

Deconvolution

Convolution is an unavoidable error that occurs during AFM imaging. It causes the lateral size of objects to appear larger than in reality and is due to the finite size of the cantilever tip and the object being imaged.[42] This means that the measured widths of polymer aggregates are initially inaccurate. Therefore, a technique known as deconvolution must be carried out to achieve an accurate value for the lateral size of the polymer features. In our previous study of

poly(styrene-co-butadiene) on a mica surface, a deconvolution method was presented for calculating the real radius of spherical cap shaped aggregates.[36] This equation can be modified to give the real width, W_{cap}, of spherical cap shaped aggregates:

$$W_{cap} = 2\sqrt{\frac{2V_r - \frac{1}{3}\pi h^3}{\pi h}} \quad (2)$$

Where V_r is the real volume of the caps and h is the height of the caps. The polymer morphology on the graphite surface was far more variable, which means additional deconvolution methods were required. At some concentrations, the polymer formed more elongated structures on the surface such as ribbons or networks. Cross-sections were taken of these structures to measure their apparent widths, W_a. In order to measure the real width, W_{el}, of these elongated structures, a method was adopted from Fung et al.[43] who developed a technique of deconvolution for oligopeptides on a surface. Where h is the height of the structures, and R_t is the radius of the AFM tip:

$$W_{el} = W_a - 2\sqrt{h(2R_t - h)} \quad (3)$$

This method was adopted for our own system, as the oligopeptides in Fung et al. study had similar morphologies to the polymer ribbons or networks formed on the graphite surface. Therefore, giving a good estimation of the real lateral size of the polymer structures.

Individual polymer aggregates (nanoislands) also formed on the graphite. However, they were not uniform as some were spherical cap shaped and others were more elongated. In order to determine which deconvolution method was appropriate for the individual aggregates, their eccentricity ε, was measured to identify how circular or elliptical an aggregate was. The eccentricity was defined as:

$$\varepsilon = \sqrt{1 - \frac{b^2}{a^2}} \quad (4)$$

Where b is length of the minor axis (width), and a is the length of the major axis (length). When ε ranged from 0 – 0.6, the droplet could be considered a spherical cap and Eq.1 was used. When ε ranged from 0.6 – 1, the method used in Eq.2 was better suited.

The number of chains in each aggregate was then found by calculating the volume of a single chain, V_c, from its molecular weight, M_n, and density, ρ:

$$V_c = \frac{(\frac{M_n}{N_A})}{\rho} \quad (5)$$

The density of the poly(styrene-co-butadiene) copolymers were assumed to be equal to their bulk values (~0.95 g/cm^3).[40] The total real volume, V_r was then divided by the volume of a single polymer chain to provide a value of how many chains made up each aggregate.

Contact Angle Measurements

The contact angles of the polymer features were obtained by using AFM. The following equation was adopted to calculate the contact angle, θ, of the spherical cap shaped nanodroplets:[44]

$$\frac{\theta}{2} = \tan^{-1}(\frac{2h}{W_{cap}}) \quad (6)$$

However, polymer morphology on the graphite surface was variable. Therefore, in order to achieve reasonable contact angle values for the less uniformly shaped aggregates, multiple line scans were taken along the profile of each aggregate. Individually, the line scans appeared as 2D cap shaped and thus, the contact angle could be measured. The average contact angle of the multiple line scans were calculated to give an overall value for each aggregate. The ESI contains profile plots of typical polymer features at each concentration

fitted to 2D spherical caps.

Data Analysis

In each AFM image, there were many individual polymer features that formed on the graphite. Therefore, on the graphs in Figures 4 – 5 and 9 – 10, each point represents an average value of feature width, height, contact angle and number of chains per aggregate. Included in the ESI are typical histograms showing the distributions of polymer morphology at specific concentrations and molecular weights. Many of the histograms do not exhibit a normal distribution, therefore including bars on the graphs that represented standard deviation were not suitable for the data. Instead, the bars on the graphs show the overall range of values for the array of features at a given parameter. This means the distributions of polymer morphology could be thoroughly examined, and factors such as polydispersity of feature size were compared at varying parameters. Error bars associated with the error using AFM were omitted as they were at the size or smaller than the symbols used. Fast Fourier transforms (FFT) were utilised to calculate the peak-to-peak distances of the polymer network features. Details of the FFT analysis can be found in the ESI. Analysis of the topography of the graphite surface is also included in the ESI.

Results and Discussion

AFM Images and Profiles

Figures 1 – 3 show representative AFM height images of the poly(styrene-co-butadiene) samples on graphite, at each concentration and molecular weight. Line scan plots showing the surface profiles of the images are also included. Generally, the line scans were taken as a full horizontal line across an image. The black lines on the profile plots relate to a scan which was

taken across the upper part of the image, whilst the red lines relate to a scan across the lower part of the image. At some lower concentrations, bars in the AFM images represent the area where the line scan took place.

M_n = 46 kg/mol

Figures 1A and 1B show that at 3c*, the polymer formed a mostly continuous thin film. Some dewetting occurred, creating circular holes in the film with depths ranging from 2.4 nm to 20 nm. Circular aggregates were also observed on the film with heights ranging from 37 nm to 41 nm. Figures 1C and 1D show that at 1c*, a very coarse polymer network is formed on the graphite. The peak-to-peak distances of the network features ranged from 867 nm to 7.4 μm, while their heights ranged from 16 nm to 79 nm. Figures 1E and 1F show a very fine continuous network at 0.1c*, with peak-to-peak distances and heights of 199 nm to 805 nm and 2.4 nm to 9.7 nm, respectively. The range of values were much smaller than the coarser network formed at 1c*. Figures 1G and 1H show that at 0.01c*, asymmetrical polymer nanoislands formed with widths and heights ranging from 16 nm to 561 nm and 0.5 nm to 18 nm, respectively. Figures 1I and 1J show that at 0.001c*, polymer nanoribbons formed at the surface. Nanoribbons are extremely small polymer features, which contain very few chains. They have an elongated shape and very low height values due to the strongly adsorbing graphite surface. The nanoribbons had widths and heights ranging from 5.3 nm to 80 nm and 0.3 nm to 0.7 nm, respectively.

Mn = 86 kg/mol

Figures 2A and 2B show that at 3c*, a mostly continuous thin film formed with a few small holes with depths ranging from 1.3 nm to 9 nm. There were several aggregates present with

heights ranging from 20 nm to 42 nm. Figures 2C and 2D show that at 1c*, a coarse continuous network is formed with peak-to-peak distances and heights ranging from 1.0 μm to 2.1 μm and 11 nm to 78 nm, respectively. Figures 2E and 2F show that at 0.1c*, a finer continuous network is formed with peak-to-peak distances and heights of 125 nm to 301 nm and 0.9 nm to 3.6 nm, respectively. Figures 2G and 2H show that at 0.01c*, irregular nanoislands formed with widths and heights ranging from 2.8 nm to 839 nm and 1.6 nm to 53 nm, respectively. Figures 2I and 2J show that at 0.001c*, nanoribbons formed with widths and heights ranging from 23 nm to 107 nm and 0.2 nm to 0.8 nm, respectively.

M_n = 355 kg/mol

Figures 3A and 3B show that at 3c*, a thin film formed with some significant amounts of dewetting characterised by holes with raised rims around their circumference. The depths of these holes ranged from 2.0 nm to 32 nm. There were numerous circular aggregates on the film with heights ranging from 6.5 nm to 225 nm. Figures 3C and 3D show that at 1c*, a coarse network is formed with peak-to-peak distances and heights ranging from 485 nm to 728 nm and 6.3 nm to 22 nm, respectively. Figures 3E and 3F show a finer continuous network at 0.1c*, with peak-to-peak distances and heights ranging from 275 nm to 441 nm and 1.1 nm to 3.3 nm, respectively. Figures 3G and 3H show that at 0.01c*, nanoislands formed with widths and heights ranging from 27 nm to 353 nm and 2.1 nm to 5.3 nm, respectively. Figures 3I and 3J show that at 0.001c*, the features were much less defined than the nanoribbons that formed at lower molecular weights. The features widths and heights ranged from 8.3 nm to 46 nm and 0.2 nm to 2.0 nm, respectively.

Concentration Effects

Size Distribution of Polymer Features

Figure 4 shows how the width of the polymer features varied with concentration for each molecular weight. The average width of the polymer features increased in small increments between 0.001c* and 0.1c*. The nanoribbons that formed at 0.001c* always had average width values less than 50 nm. Whereas, the networks that formed at 0.1c* all had average width values greater than 170 nm. We consistently observed an abrupt increase in feature width between 0.1c* and 1c* for all molecular weights investigated. At 1c*, the polymer morphology changed from a fine continuous network to a much coarser one, and the average width values varied from approximately 600 to 3000 nm. Furthermore, the range of values for the coarse networks at 1c* were considerably larger than the three lower concentrations. The coarse networks had a polydisperse width distribution, whereas at 0.001c*, the width distribution was much more monodisperse. For the 86 kg/mol sample, the nanoislands that formed at 0.01c*, also had a more polydisperse width distribution.

Figure 5 shows the relationship between feature height and concentration at each molecular weight. At 0.001c*, the nanoribbons had small average height values (<1nm) and a monodisperse height distribution. At 1c*, the average height values were significantly larger than the three other concentrations and the distribution was more polydisperse. However, the average height of the polymer features did not increase consistently with concentration. This is demonstrated at 0.01c*, where the asymmetrical nanoislands had larger average height values than the continuous networks that formed at 0.1c*. Furthermore, the range of values at 0.01c* were always larger than at 0.001c* and 0.1c*. At each concentration, the polymer features had much greater width values than height values. This is to be expected as the

polymer strongly adsorbs onto the graphite surface.

The nanoribbons that formed at 0.001c* are of particular interest due to their extremely small average height values of 0.44 nm, 0.42 nm, and 0.65 nm for the 46 kg/mol, 86 kg/mol, and 355 kg/mol samples, respectively. These values are comparable to the characteristic height of a single polymer chain adhered to a surface (~0.4 nm).[45,46] This suggests that at this concentration, many of the polymers were adsorbed onto the graphite surface in a monolayer. However, the average widths of the nanoribbons were 38 nm, 48 nm, and 22 nm for the 46 kg/mol, 86 kg/mol and 355 kg/mol samples, respectively. These values are far greater than the width of a single polymer chain. This suggests that at the graphite surface, the polymer chains either fold against themselves, or many chains aggregate side by side to create a nanoribbon with monolayer thickness.

Thin Film Morphology

At the highest concentration (3c*), mostly continuous thin films were formed on the graphite at each molecular weight. AFM images and cross-sectional profile plots of holes in the films were used to calculate values of film thickness. Details of this analysis, in addition to a typical phase image and profile plot are included in the ESI. The film thickness values were 20 nm and 32 nm for the 46 kg/mol and 355 kg/mol samples, respectively. An accurate measurement of film thickness could not be obtained for the 86 kg/mol sample as the dewetted holes imaged were small. This meant we could not be certain that the holes exposed the graphite surface. However, we can conclude that the films had a thickness of ≥ 9 nm. It was expected that the polymer films would be continuous and no dewetting would be observed on the surface. This is because the effective Hamaker constant of the system was

negative and the films had larger thickness values than the polymers radius of gyration (R_g) (see ESI for details).[47,48] However, this was not the case and we observed the formation of holes in the films created by dewetting through rapid nucleation caused by impurities, thermal fluctuations or spinodal decompositon.[49,50] The holes in the films were either small (Figure 1A), or larger with raised rims around their circumference (Figure 3A). After 16 – 72 hours at ~ 55˚C above their T_g, the polymers did not form equilibrium structures on the graphite. This shows that the films were in a state of metastable equilibrium. This metastable state could be caused by interface effects and surface confinement.[9,51]

To further probe the dewetting behaviour of the thin films, the relationship between the diameter of the dewetted holes and the height of the rims around the circumference of the holes was investigated. A linear relationship between hole diameter and rim height was observed by G. Reiter using almost glassy polystyrene thin films on a highly nonwettable substrate annealed close to their T_g.[52] Reiter explained that this linear trend, alongside the asymmetric shape of the rim, strongly suggested that the polymer did not flow like a viscous liquid. Instead, driving capillary forces were responsible for plastically deforming the film, creating dewetting. Furthermore, under these experimental conditions, the reptation time of the polymer was over a year, which means viscous flow could not occur in the experimental time scale.

Figure 6 shows the relationship between hole diameter and rim height at 3c* for the 355 kg/mol sample. The graph shows that there is a linear relationship between hole diameter and rim height for the poly(styrene-co-butadiene) thin film at 355 kg/mol in our study, despite the polymer being deposited onto a strongly adsorbing substrate. Furthermore, the shape of the

rims were asymmetric, with sloped rear sides and steep insides (see Figure S-13 in ESI). This behaviour was only observed for the 355 kg/mol sample, as the films were in a more advanced state of dewetting due to an increased film thickness. This led to larger holes and the formation of raised rims. The slope of the graph in Figure 6 relates to the material properties of the system including film thickness, viscosity in the film, and the coefficient of friction at the interface.[53] This is an interesting result, as the 355 kg/mol polymer was considerably above its T_g at room temperature, which can account for the viscous fingering observed in the films (Figure 3A), but cannot account for the above observations which are usually attributed to plastic deformation.[52] Whilst we cannot conclusively say that the film had experienced plastic deformation, the observed dewetting behaviour does indicate this. Therefore, the polymer films may have exhibited both viscous dewetting and plastic deformation. This could have been influenced by an increase in the effective T_g of the adsorbed polymers due to confinement effects at the interface.[54]

In our previous study of poly(styrene-co-butadiene) on a mica surface, the polymer thin films also exhibited a linear relationship between rim height and hole diameter, and asymmetrically shaped rims.[36] This was again indicative of both plastic deformation and viscous dewetting. However, there are some significant differences in the dewetting behaviour of the thin films on each substrate. On the mica surface, the dewetted holes were large with maximum diameters of ~ 15 μm. Whereas, under the same experimental conditions on the graphite surface, the dewetted holes were smaller with diameters up to only ~ 3 μm. Additionally, on the mica substrate, the thin films had much larger viscous fingering patterns. This suggests that strong adsorption of the polymers to the graphite surface causes a decrease in the rate of hole growth by preventing movement of the chains. Therefore, the dewetted holes on the graphite were in the early stages of dewetting, and thus, there was a reduced accumulation of

polymeric material around their circumference which led to limited viscous fingering patterns.

Distinct Ordering of Polymer Nanostructures

Figure 7A shows an AFM phase image for the 86 kg/mol polymer at 0.001c*. The image shows a series of nanostructures on the surface created through self-assembly of the polymer, with specific ordering at intervals of 60˚. This is further demonstrated in the histogram in Figure 7B, which exhibits distinct peaks at intervals of 60˚. This shows that the polymer chains orientated themselves to reflect the crystalline symmetry of graphite, creating an ordered nanopattern.[55] This behaviour has been previously observed with crystalline polymers, such as polyethylene. While graphite has a hexagonal crystalline structure and polyethylene has an orthorhombic crystal structure;[56,57] the distance of the next nearest neighbour of the graphite lattice (2.46Å) is similar to the length of the c-axis in a polyethylene crystal cell (2.55Å).[32] This encourages epitaxial nucleation on the graphite surface resulting in an ordered polymer morphology. The effect has also been observed on graphite using polymers with pendant alkyl chains. In these instances, the 1,3-methylene group distance (2.51Å) in trans alkyl chains matches the distance of the next nearest neighbour of the graphite lattice, with adsorption of the alkyl chains onto the graphite surface driving the distinct ordering.[33–35]

Previous research has demonstrated that observing distinct ordering on graphite is uncommon when using a linear amorphous polymer. Chen et al.[58] observed specific ordering with the amorphous homopolymer poly(4-vinylpyridine) (P4VP) on graphite. Chen et al. study demonstrated that this epitaxy-like orientation in dewetted thin films of P4VP occurred only

when the height of the nanostructures was less than 5 nm. For structures with heights greater than 5 nm, no evidence of ordering was observed. Chen et al. cited this epitaxy-like behaviour to the pyridine-group distribution matching the graphite lattice and nucleation at mosaic-block boundaries.[58] To our knowledge, the investigation by Chen et al. is the only study to observe the distinct ordering of an amorphous homopolymer on graphite. Specific ordering on graphite has never been observed with a linear amorphous copolymer.

Figures 7B and 8 show the angle (relative) frequency distributions for polymer features that form at 0.001c* to 1c*. Below the overlap concentration (0.001c* to 0.1c*), clear peaks are present in the histograms at intervals of 60˚. At the overlap concentration (1c*), there are still some peaks at 60˚ intervals but they are not so distinct. Table 1 shows the percentage of features measured that are arranged at 60˚ intervals and the average height values, at each concentration. At the lowest concentration (0.001c*), the ordering was very precise and 96% of the features measured were arranged at intervals of 60˚. At 0.01c* and 0.1c*, 69% and 68% of the features measured were arranged at angles of 60˚, respectively. At 1c*, the average height of the features was 38 nm and 48% of the features measured were arranged at 60˚ intervals. This ordering may be due to π-π stacking interactions between the poly(styrene-co-butadiene) and the graphite surface. This intermolecular interaction appears to drive ordering in samples at higher concentrations, as some ordering is observed for nanostructures with height values much greater than previously reported with amorphous polymers.[58]

The π-π stacking interactions may be more favourable between polystyrene and graphite compared to polybutadiene and graphite due to the aromatic ring in the styrene unit. Thus, the nanopatterning may be driven by the ~25% styrene units in the random poly(styrene-co-

butadiene) copolymers. Therefore, the morphology of polystyrene and polybutadiene homopolymers on graphite was studied to investigate the influence of aromatic rings in creating this ordering in polymers at the nanoscale. AFM height images and orientation (relative) frequency distributions for the polystyrene and polybutadiene homopolymers at each concentration investigated can be found in the ESI. The homopolymers had similar molecular weights to the poly(styrene-co-butadiene) samples and were deposited onto graphite using the same experimental methods. The polystyrene formed a continuous network and asymmetrical nanoislands on the surface. The average height of the network was 1.3 nm and 42% of the features measured were orientated at 60˚ intervals. The average height of the asymmetrical nanoislands was 1.5 nm and 42% of the features measured were orientated at 60˚ intervals. For nanostructures with similar height values, we observed significantly more ordering for poly(styrene-co-butadiene) than polystyrene. This is somewhat surprising, as polystyrene contains a greater number of aromatic rings and thus the potential for increased π-π stacking. Yang et al.[59] demonstrated that chain flexibility can affect the interactions between polymers and CNT's. In our study, the poly(styrene-co-butadiene) chains are more flexible than polystyrene, and the aromatic rings are arranged randomly along the chain. 1H NMR conducted by the provider examined the monomer distribution in the chains. It was demonstrated that there was a >95% probability that the styrene blocks in the chains had lengths of 1 - 3 monomer units (the same applies to butadiene monomers). This shows that the random copolymers did not contain large blocks of either styrene or butadiene monomer units. Therefore, the random distribution of the styrene units may have prevented *in-chain* π-π stacking interactions, and gave the chain enough flexibility to allow the rings to align on the surface and maximise π-π stacking with the graphite. In polystyrene, the aromatic rings are adjacent to each other, and the chain is less flexible. This prevents free movement of the rings and means that collectively, they cannot align to maximise π-π stacking with the surface.

The polybutadiene homopolymer formed a semi-continuous film and asymmetrical nanoislands at the concentrations investigated. The average height of the semi-continuous film was 2.5 nm and 42% of the features measured were orientated at angles of 60˚. The average height of the asymmetrical nanoislands was 3.5 nm and 41% of the features measured were orientated at 60˚ intervals. The heights of the polybutadiene structures were very similar to that of the poly(styrene-co-butadiene) networks and islands. However, the poly(styrene-co-butadiene) experienced a significantly greater degree of ordering on the surface. This demonstrates that although polybutadiene is flexible, the lack of aromatic rings prevents a high degree of ordering due to limited π-π stacking. These results suggest that the ordering of amorphous polymers on a carbon surface is heavily influenced by both chain flexibility and the proportion of aromatic rings in a chain. This ordering effect at a carbon surface could prove useful in nanopatterning applications.

Molecular Weight Effects

Size Distribution of Polymer Features

Figures 9 and 10 compare molecular weight against feature width and height at varying concentrations on the graphite surface. The number of chains per aggregate could only be examined at 0.01c* as this was the only concentration where individual nanoislands formed.

Figures 9A and 9B show how the width of the network features that formed at 1c* and 0.1c* varied with molecular weight. The two graphs show similar trends as the average width values of the networks consistently decreased between 46 kg/mol and 86 kg/mol, and then stayed at similar values for the 355 kg/mol sample. Therefore, the networks had the largest

width values when the polymer chains were the shortest. Additionally, the width distributions were largest for the 46 kg/mol sample at both 1c* and 0.1c*. Figure 9C shows that at a concentration of 0.01c*, where individual nanoislands formed, feature width remained fairly constant with increasing molecular weight. The average width value of the nanoislands only varied by 14 nm across all three molecular weights, although the range of values was lowest for the 355 kg/mol sample. Figure 9D shows that the average width of the polymer nanoribbons formed at 0.001c* was lowest at 355 kg/mol, whilst the 46 kg/mol and 86 kg/mol samples had similar values of 39 nm and 48 nm, respectively. The 355 kg/mol sample also had the smallest range of values, whereas the two lower molecular weights had similar width distributions.

The graphs in Figures 10A and 10B show similar trends as feature height decreased with increasing molecular weight for the networks formed at both 1c* and 0.1c*. Furthermore, the height distribution was lowest at 355 kg/mol at both concentrations. Figure 10C shows that at 0.01c*, the height values of the nanoislands generally remained constant as molecular weight was increased. The average height value only varied by 9 nm across all three molecular weights. However, the 355 kg/mol sample had a considerably smaller height distribution than the two lower molecular weight samples. Figure 10D shows that the height of the nanoribbons that formed at 0.001c* were very similar for the 46 kg/mol and 86 kg/mol samples which had average values of 0.44 nm and 0.42 nm, respectively. The 355 kg/mol sample had a marginally larger average height value (0.65 nm) and the largest height distribution. Figures 9C and 10C show that the heights and widths of the nanoislands formed at 0.01c* remained mostly constant with variations in molecular weight. Therefore, as molecular weight increased and the polymer chains became longer, it took fewer chains to assemble into aggregates of the same size. The graph demonstrating this trend can be found

in the ESI.

For the networks that formed at 1c* and 0.1c*, generally the average size of the polymer features decreased with increasing molecular weight. However, for the nanoislands and nanoribbons that formed at 0.01c* and 0.001c*, the size of the features remained similar when molecular weight increased. The reason for this varying relationship between molecular weight and nanostructure size is due to adsorption effects. Chains with higher molecular weights tend to maximise their contact with the surface, so that the sum of the adsorption energy gained from the adsorbed monomers is greater than the entropic loss.[40,60] This means it is favourable for the longer chains to maximise contact with the surface, despite the loss of entropy due to confinement.[61] However, for the lower molecular weight chains, it is less energetically favourable for them to adsorb to the surface, as the sum of the adsorption energy gained may not exceed the entropic loss. Consequently, the shorter chains will stay away from the surface in a more unperturbed state, meaning that larger features are more likely.[40] This is prevalent during the final stages of evaporation where the shorter chains can desorb more easily following the instabilities of the solvent and create larger features, whereas the longer chains are strongly bound to the surface. This behaviour explains why at higher concentrations we observed larger polymer features at lower molecular weights. However, at lower concentrations, the size of the polymer features remained fairly constant with increasing molecular weight. This is because there were fewer chains present at the surface during solvent evaporation, which means the chains were likely to be adsorbed onto the graphite surface regardless of molecular weight.

The relationship between feature size and molecular weight on the graphite surface is very different to when the poly(styrene-co-butadiene) was deposited onto mica. On the mica substrate, the average size of the polymer features generally increased with increasing molecular weight at each concentration.[36] This is because the poly(styrene-co-butadiene) weakly adsorbs onto the mica surface which means that the chains do not experience the same loss of entropy and gain in adsorption energy due to confinement effects. Instead, it is favourable for the chains to minimise surface energy and aggregate into spherical caps, regardless of molecular weight. This behaviour leads to fewer but larger aggregates on the mica surface at higher molecular weights.

Thin Film Morphology

The 355 kg/mol polymer films had greater thickness values than the 46 kg/mol films. Furthermore, the 355 kg/mol thin films appeared to be in a more advanced state of dewetting, exhibiting larger holes (diameters up to 3 μm) with distinct raised rims around their circumferences. The 46 kg/mol films had smaller holes (diameters up to 2 μm) and no raised rims. The apparent reason for this increased dewetting for the 355 kg/mol sample is not directly due to molecular weight effects. Previous investigations have demonstrated that the rate of dewetting for thin films with similar thicknesses did not change with variations in molecular weight.[52] The likely reason for this dewetting behaviour appears to be due to a greater initial film thickness in the 355 kg/mol sample. A greater amount of dewetting in polymer thin films with a larger thickness has been reported in the literature, as well as in our previous work.[36,62,63] Many factors are thought to be responsible for creating this relationship including the magnitude of the van der Waals force acting on a film which increases with increasing film thickness and thus creates a faster rate of dewetting.[64] However, the reason

why the 355 kg/mol sample had a greater film thickness could be due to a higher molecular weight which allowed more polymeric material to remain on the graphite substrate during spin coating via increased viscosity and entanglements.[36] This suggests that although molecular weight effects did not directly causing an increase in dewetting, they were indirectly influencing this behaviour by creating films with larger thicknesses.[65]

Contact Angle Effects

The contact angles of the polymer features were investigated in relation to feature width. It was found that there was no specific size dependence on the polymer contact angle and the average contact angle values were all small (< 9˚). Across the nanoscale, the average contact angle values were fairly constant and only fluctuated by 4.2˚, 5.4˚, and 2.9˚ for the 46 kg/mol, 86 kg/mol, and the 355 kg/mol samples, respectively. This is different to the results observed when the polymer was deposited onto mica, where the contact angle of the nanodroplets were found to be extremely size dependent.[36] The graphs showing how contact angle of the polymer features varied with feature width are included in the ESI.

Milchev et al.[66] simulations study demonstrated that when polymer/substrate adhesion was strong, the contact angle of polymer droplets at a surface remained fairly constant as their size was reduced across the nanoscale. This behaviour was attributed to the droplets having no influence from line tension effects, due to strong polymer/substrate adhesion. Despite having a more variable polymer morphology, our experimental results are in line with Milchev et al. simulations. There was strong polymer/substrate adhesion, and the polymer contact angle remained fairly constant across the nanoscale. This may provide experimental confirmation of Milchev et al. simulations study regarding the fairly controversial subject of

line tension. Furthermore, any possible influence on the polymer contact angle caused by an increased effective elastic modulus due to confinement effects was also prevented by the strong polymer/substrate adhesion.[36,67] Our results from studies examining polymer morphology on graphite and mica demonstrate that the substrate physicochemical properties and strength of adsorption between the polymer and the substrate are extremely influential in determining how the contact angle of polymer nanodroplets varies with droplet size.[36]

Summary and Conclusion

We have carried out a comprehensive study on the fundamental behaviour of poly(styrene-co-butadiene) random copolymers on a graphite surface at the nanoscale. Above the overlap concentration, mostly continuous thin films formed which experienced partial dewetting. This is significant as the polymers have a very low T_g, and therefore, it would be expected for equilibrium structures to form on the strongly absorbing graphite surface. Instead, dewetting occurred demonstrating that the polymers were in a state of metastable equilibrium. This could be caused by interface and confinement effects.

A linear relationship between the diameter of the dewetted holes and the height of their raised rims was also observed, in addition to evidence of viscous fingering. This demonstrated that the thin films exhibited both viscous and plastic properties. As concentration was reduced, networks, asymmetrical nanoislands, and nanoribbons formed on the graphite. There was variability in feature size at different concentrations which appeared to be due to the changes in polymer morphology from continuous networks to nanoislands and nanoribbons.

Precise ordering of the polymer chains was observed at the lowest concentration, creating epitaxy-like features on the surface arranged at 60˚ intervals. This demonstrated that through π-π stacking interactions; poly(styrene-co-butadiene) can self-assemble via spin coating to reflect the crystalline structure of the graphite and create ordered nanopatterns. Furthermore, we have shown that at higher concentrations (up to 1c*), polymer morphology also experiences some degree of ordering in nanostructures with average heights up to 38 nm. This demonstrated that the π-π stacking interactions between the copolymer and the graphite are highly favourable. To further investigate the interactions between our copolymer and the graphite, the experiments were repeated using polybutadiene and polystyrene homopolymers. Both homopolymers experienced significantly less ordering on the surface compared to poly(styrene-co-butadiene). We can conclude that a high degree of ordering was observed in poly(styrene-co-butadiene) due to the aromatic rings being randomly spaced along a flexible chain which maximises π-π stacking interactions.

The 355 kg/mol thin film exhibited a greater amount of dewetting than the 46 kg/mol thin film. The likely reason for this is that the 355 kg/mol sample had a larger film thickness which increased the rate of dewetting. For the networks that formed at 1c* and 0.1c*, the size of the features were generally largest at the lowest molecular weight. This is because the shorter chains will be less likely to adsorb to the surface and remain in an unperturbed state, due to limited gains in adsorption energy from binding to the surface. However, at 0.01c* and 0.001c*, the size of the nanoislands and nanoribbons remained more constant with increasing molecular weight. This is because at lower concentrations, there were fewer chains at the surface during solvent evaporation. This means at every molecular weight, it is more probable for the individual chains to adsorb to the surface.

We have demonstrated experimentally that the contact angle of the polymer features remained fairly constant with varying feature size. These results are in line with previous simulation experiments, and show that the strong polymer/graphite adhesion prevents any influence on contact angle, from line tension or an increased effective elastic modulus.

We have provided a greater understanding of how polymers behave at a carbon surface at the nanoscale. This could prove beneficial in optimising the design and manufacturing processes of composite materials, and lead to improvements in their bulk physicochemical properties.

Supporting Information

Conversion of solution concentration between c* and mg/ml; fitting polymer features to spherical caps; feature size distributions; FFT analysis; graphite substrate topography; film thickness calculations; radius of gyration and effective Hamaker constant calculations; ordering analysis of polystyrene and polybutadiene; number of chains per aggregate against molecular weight; contact angle against feature width.

Author Information

Corresponding Author

* E-mail vasileios.koutsos@ed.ac.uk; Tel.: +44 (0)131 650 8704; Fax: +44 (0)131 650 6551.

Notes

The authors declare no competing financial interest.

Acknowledgements

We would like to thank Michelin and Marc Couty for providing the polymer samples and carrying out GPC and DSC measurements. We acknowledge the financial support of the EPSRC and the SOFI CDT (Grant Ref. No. EP/L015536/1).

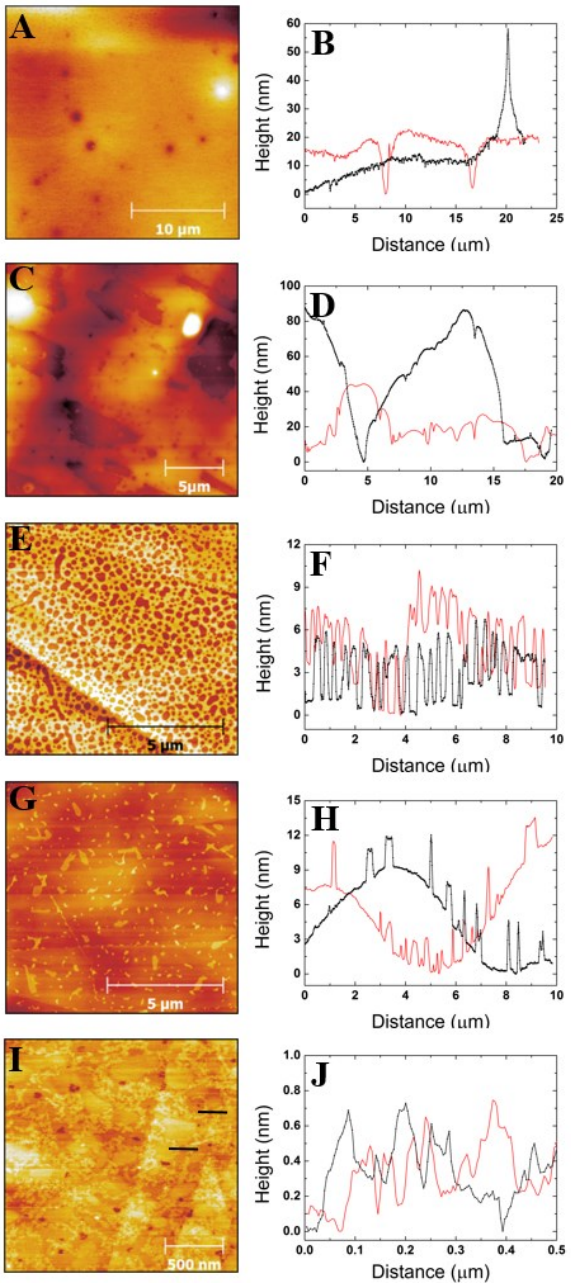

Figure 1: AFM height images and profile plots for the 46 kg/mol poly(styrene-co-butadiene) sample at varying concentrations on a graphite surface. The profile plots correspond to horizontal line scans across the images, unless a bar is present, which corresponds to where the profile plot has taken place. (A) 3c* = 17.43 mg/ml, thin film (B) profile plots at 3c*, (C) 1c* = 5.81 mg/ml, network (D) profile plots at 1c*, (E) 0.1c* = 0.581 mg/ml, network (F) profile plots at 0.1c*, (G) 0.01c* = 0.0581 mg/ml, nanoislands (H) profile plots at 0.01c*, (I) 0.001c* = 0.0058 mg/ml, nanoribbons (J) profile plots at 0.001c*.

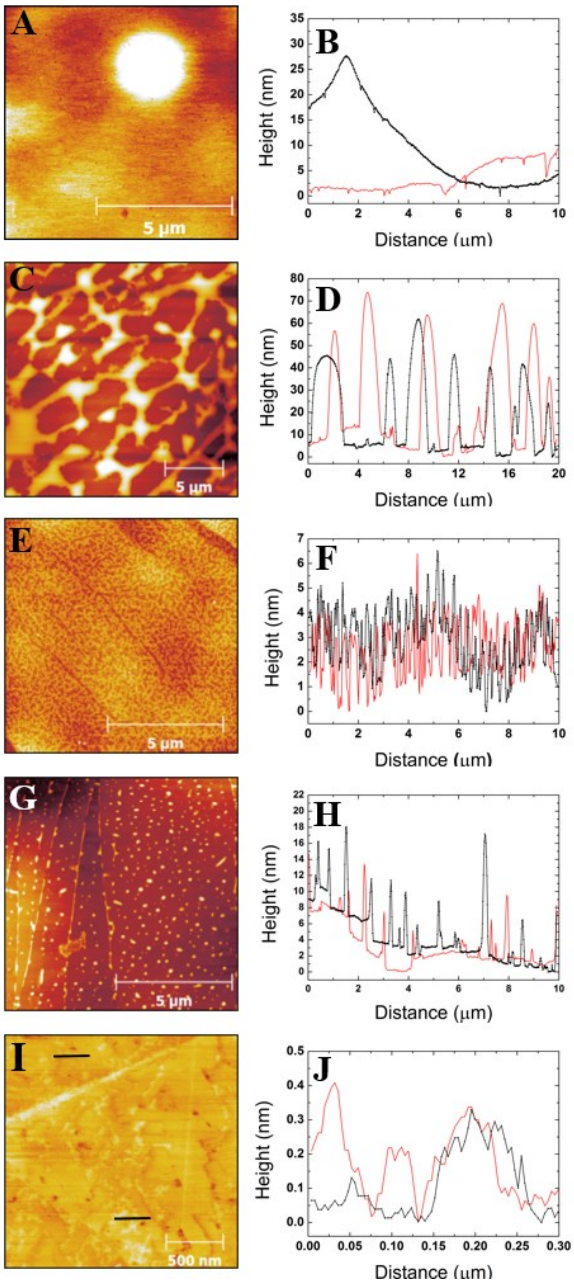

Figure 2: AFM height images and profile plots for the 86 kg/mol poly(styrene-co-butadiene) sample at varying concentrations on a graphite surface. The profile plots correspond to horizontal line scans across the images, unless a bar is present, which corresponds to where the profile plot has taken place. (A) 3c* = 11.13 mg/ml, thin film (B) profile plots at 3c*, (C) 1c* = 3.71 mg/ml, network (D) profile plots at 1c*, (E) 0.1c* = 0.371 mg/ml, network (F) profile plots at 0.1c*, (G) 0.01c* = 0.0371 mg/ml, nanoislands (H) profile plots at 0.01c*, (I) 0.001c* = 0.0037 mg/ml, nanoribbons (J) profile plots at 0.001c*.

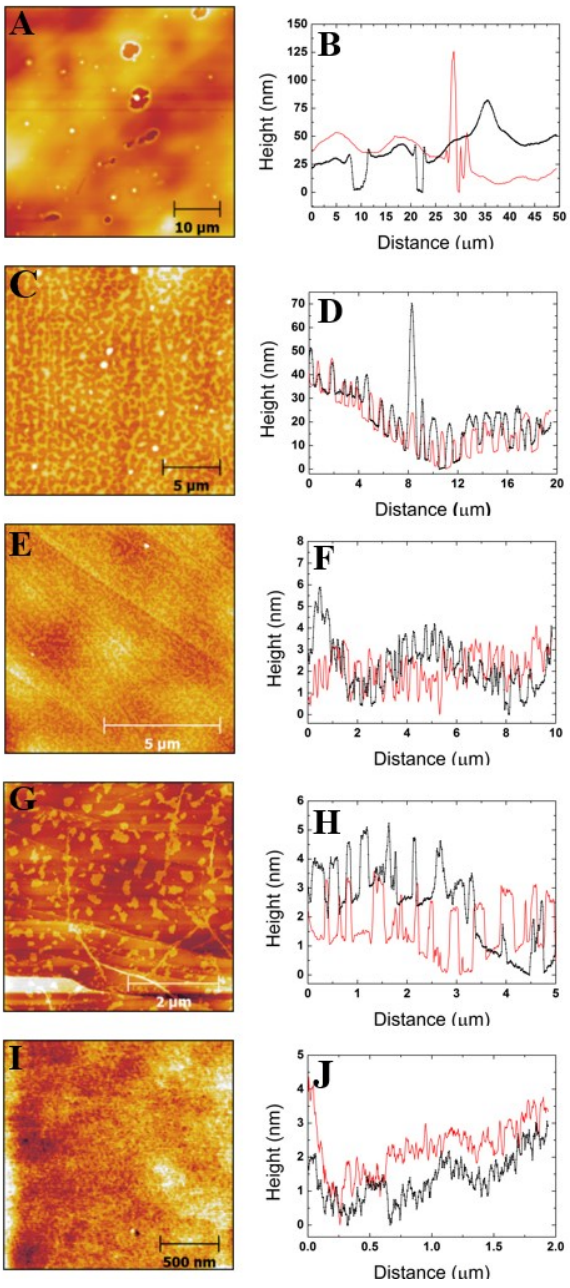

Figure 3: AFM height images and profile plots for the 355 kg/mol poly(styrene-co-butadiene) sample at varying concentrations on a graphite surface. The profile plots correspond to horizontal line scans across the images. (A) 3c* = 4.17 mg/ml, thin film (B) profile plots at 3c*, (C) 1c* = 1.39 mg/ml, network (D) profile plots at 1c*, (E) 0.1c* = 0.139 mg/ml, network (F) profile plots at 0.1c*, (G) 0.01c* = 0.0139 mg/ml, nanoislands (H) profile plots at 0.01c*, (I) 0.001c* = 0.0014 mg/ml, nanoribbons (J) profile plots at 0.001c*.

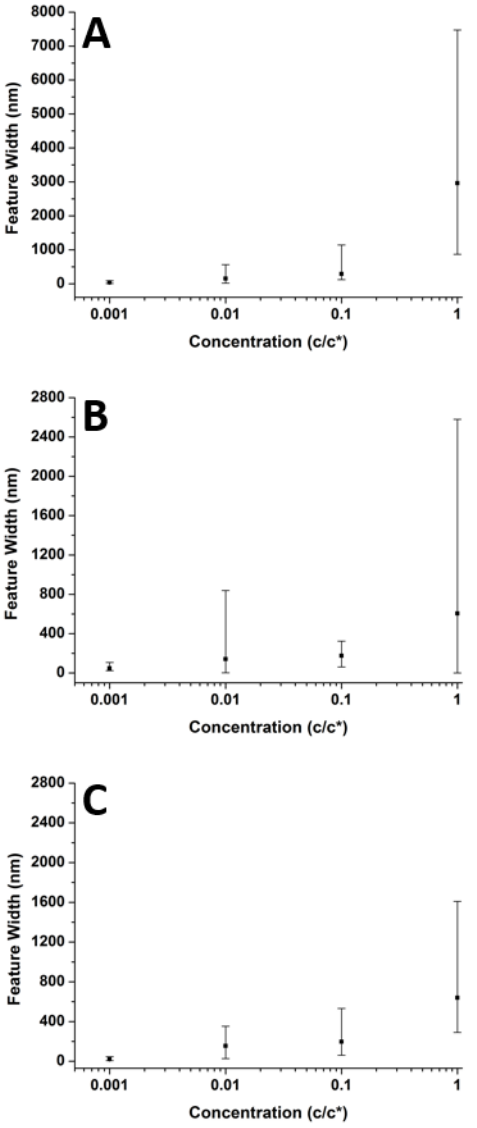

Figure 4: Graphs showing the relationship between polymer feature width and solution concentration at varying molecular weights. Each graph presents the average values and has bars which indicate the range of values. (A) M_w= 46 kg/mol, (B) M_w= 86 kg/mol, (C) M_w= 355 kg/mol.

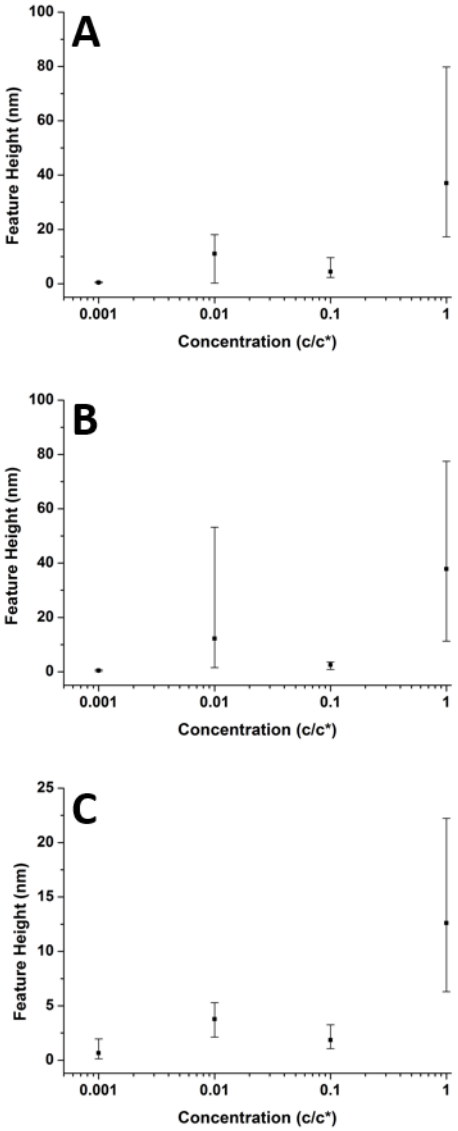

Figure 5: Graphs showing the relationship between polymer feature height and solution concentration at varying molecular weights. Each graph presents the average values and has bars which indicate the range of values. (A) M_w= 46 kg/mol, (B) M_w= 86 kg/mol, (C) M_w= 355 kg/mol.

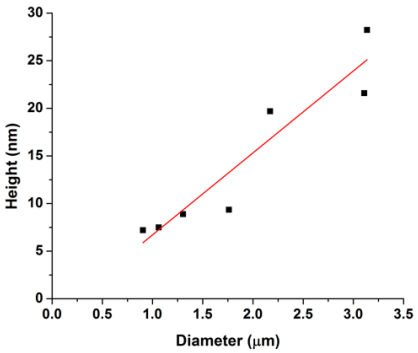

Figure 6: Graph showing the relationship between the diameter of the dewetted holes and the height of the raised rims around the circumference of the holes at 3c*. The results were taken from the 355 kg/mol sample.

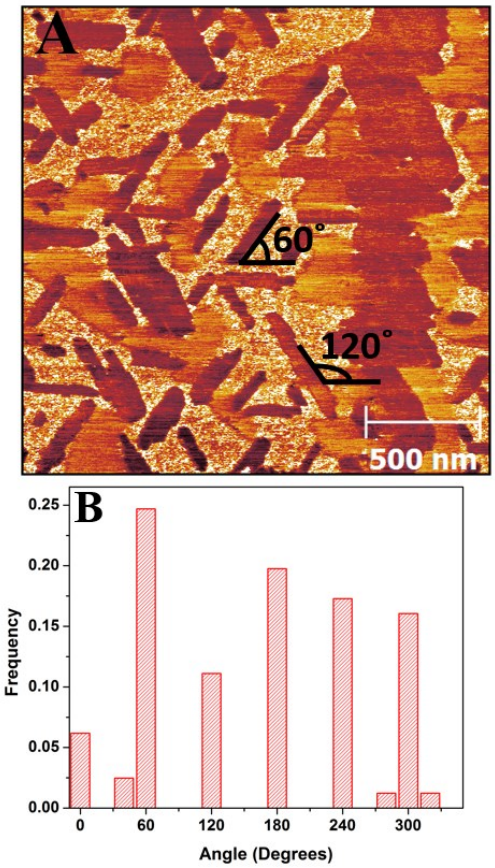

Figure 7: (A) AFM phase image of the 86 kg/mol sample at 0.001c*. Annotations show examples of the specific ordering on the surface. (B) Histogram showing the angle (relative) frequency distribution of the ordered nanostructures that form at 0.001c* for the 86 kg/mol sample.

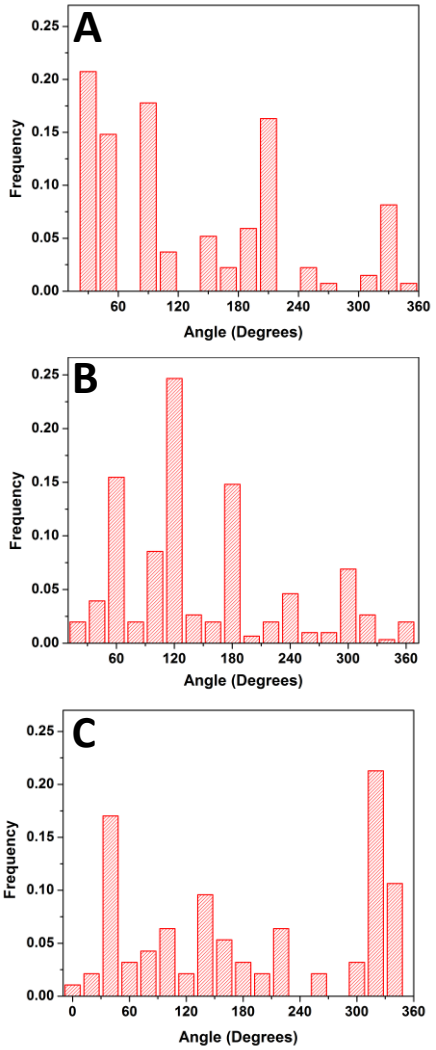

Figure 8: Histograms showing the angle (relative) frequency distributions for the polymer nanostructures at varying concentrations. (A) 355 kg/mol sample at 0.01c*, (B) 355 kg/mol sample at 0.1c*, (C) 86 kg/mol sample at 1c*.

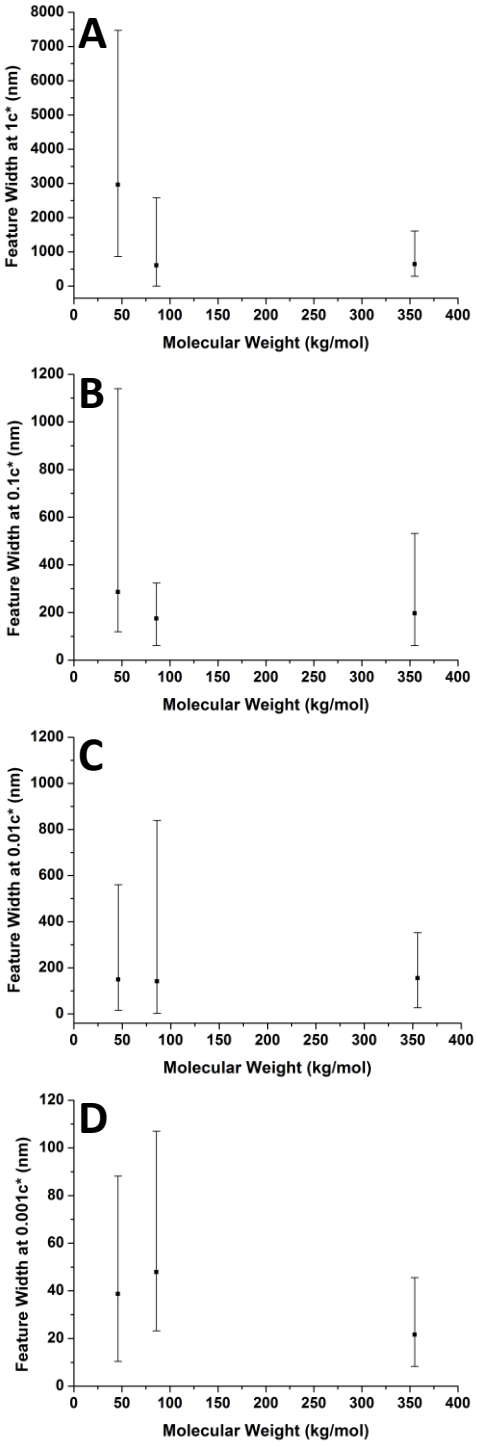

Figure 9: Graphs showing the relationship between polymer feature width and molecular weight at varying concentrations. Each graph presents the average values and has bars which indicate the range of values. (A) 1c*, (B) 0.1c*, (C) 0.01c*, (D) 0.001c*.

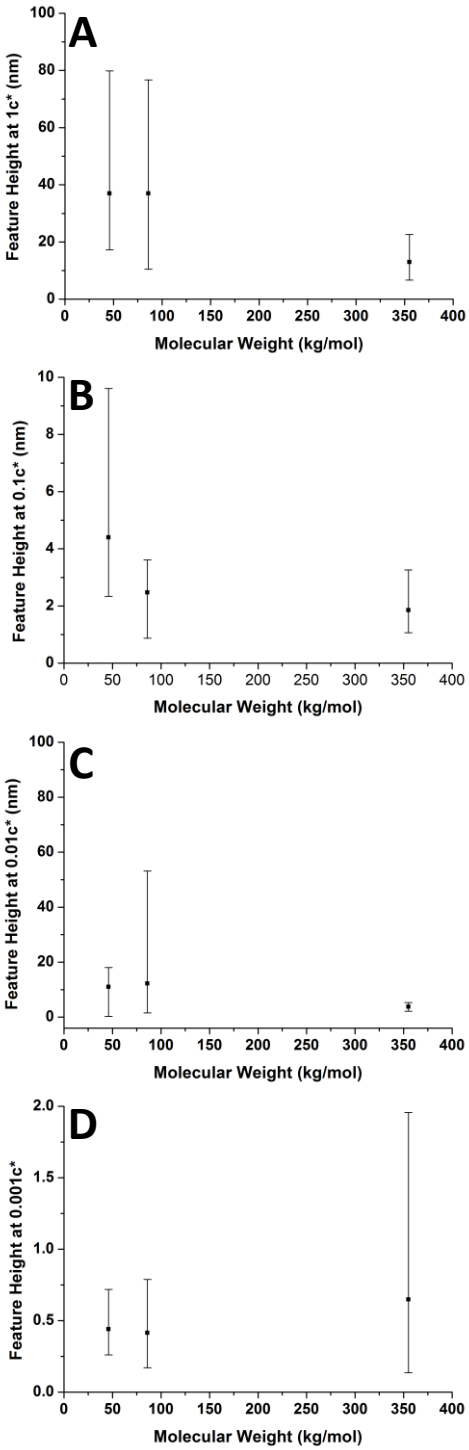

Figure 10: Graphs showing the relationship between polymer feature height and molecular weight at varying concentrations. Each graph presents the average values and has bars which indicate the range of values. (A) 1c*, (B) 0.1c*, (C) 0.01c*, (D) 0.001c*.

Table 1: Analysis of polymer ordering.

Concentration (c/c*)	Ordering at 60˚ intervals (%)	Average height (nm)
0.001c*	96	0.4
0.01c*	69	4
0.1c*	68	2
1c*	48	38

References.

(1) Nie, Z.; Kumacheva, E. Patterning Surfaces with Functional Polymers. *Nat. Mater.* **2008**, *7*, 277–290.

(2) Stuart, M. A. C.; Huck, W. T. S.; Genzer, J.; Müller, M.; Ober, C.; Stamm, M.; Sukhorukov, G. B.; Szleifer, I.; Tsukruk, V. V; Urban, M.; et al. Emerging Applications of Stimuli-Responsive Polymer Materials. *Nat. Mater.* **2010**, *9*, 101–113.

(3) Stankovich, S.; Dikin, D. A.; Dommett, G. H. B.; Kohlhaas, K. M.; Zimney, E. J.; Stach, E. A.; Piner, R. D.; Nguyen, S. T.; Ruoff, R. S. Graphene-Based Composite Materials. *Nature* **2006**, *442*, 282–286.

(4) Grosberg, A. Y.; Khokhlov, A. R. *Giant Molecules*; Academic Press: San Diego, 1997.

(5) Holbery, J.; Houston, D. Natural-Fibre-Reinforced Polymer Composites in Automotive Applications. *J. Miner. Met. Mater. Soc.* **2006**, *58*, 80–86.

(6) Mallick, P. K. Fiber-Reinforced Composites: Materials, Manufacuring, and Design; CRC Press: Boca Raton, 2007; pp 6–12.

(7) Fu, S. Y.; Feng, X. Q.; Lauke, B.; Mai, Y. W. Effects of Particle Size, Particle/matrix Interface Adhesion and Particle Loading on Mechanical Properties of Particulate-Polymer Composites. *Compos. Part B Eng.* **2008**, *39*, 933–961.

(8) Li, Y.; Hu, K.; Han, X.; Yang, Q.; Xiong, Y.; Bai, Y.; Guo, X.; Cui, Y.; Yuan, C.; Ge, H.; et al. Phase Separation of Silicon-Containing Polymer/Polystyrene Blends in Spin-Coated Films. *Langmuir* **2016**, *32*, 3670–3678.

(9) Mortazavian, H.; Fennell, C. J.; Blum, F. D. Surface Bonding Is Stronger for Poly(methyl Methacrylate) than for Poly(vinyl Acetate). *Macromolecules* **2016**, *49*, 4211–4219.

(10) Maddumaarachchi, M.; Blum, F. D. Thermal Analysis and FT-IR Studies of Adsorbed Poly(ethylene-Stat-Vinyl Acetate) on Silica. *J. Polym. Sci. Part B Polym. Phys.* **2014**, *52*, 727–736.

(11) Prucker, O.; Christian, S.; Bock, H.; Ruhe, J.; Frank, C. W.; Knoll, W. On the Glass Transition in Ultrathin Polymer Films of Different Molecular Architecture. *Macromol. Chem. Phys.* **1998**, *199*, 1435–1444.

(12) Fröhlich, J.; Niedermeier, W.; Luginsland, H.-D. The Effect of Filler-Filler and Filler-Elastomer Interaction on Rubber Reinforcement. *Compos. Part A Appl. Sci. Manuf.* **2005**, *36*, 449–460.

(13) Heinrich, G.; Klüppel, M.; Vilgis, T. A. Reinforcement of Elastomers. *Curr. Opin. Solid State Mater. Sci.* **2002**, *6*, 195–203.

(14) Chung, D. D. L. Carbon Fiber Composites; Butterworth-Heinemann: Oxford, 1994; pp 49–51.

(15) Shalin, R. E. Polymer Matrix Composites; Chapman and Hall: London, 1995; pp 132–149.

(16) Iijima, S. Helical Microtubules of Graphitic Carbon. *Nature* **1991**, *354*, 56–58.

(17) Novoselov, K. S.; Geim, A. K.; Morozov, S. V.; Jiang, D.; Zhang, Y.; Dubonos, S. V.;

Grigorieva, I. V.; Firsov, A. A. Electric Field Effect in Atomically Thin Carbon Films. *Science* **2004**, *306*, 666–669.

(18) Li, Q.; Zaiser, M.; Blackford, J. R.; Jeffree, C.; He, Y.; Koutsos, V. Mechanical Properties and Microstructure of Single-Wall Carbon Nanotube/elastomeric Epoxy Composites with Block Copolymers. *Mater. Lett.* **2014**, *125*, 116–119.

(19) Li, Q.; Zaiser, M.; Koutsos, V. Carbon Nanotube/epoxy Resin Composites Using a Block Copolymer as a Dispersing Agent. *Phys. Status Solidi A* **2004**, *201*, R89.

(20) Arash, B.; Wang, Q.; Varadan, V. K. Mechanical Properties of Carbon Nanotube/polymer Composites. *Sci. Rep.* **2014**, *4*, 1–8.

(21) Coleman, J. N.; Khan, U.; Blau, W. J.; Gun'ko, Y. K. Small but Strong: A Review of the Mechanical Properties of Carbon Nanotube-Polymer Composites. *Carbon.* **2006**, *44*, 1624–1652.

(22) Thuau, D.; Koutsos, V.; Cheung, R. Electrical and Mechanical Properties of Carbon Nanotube-Polyimide Composites. *J. Vac. Sci. Technol. B* **2009**, *27*, 3139–3144.

(23) Nagata, K.; Iwabuki, H.; Nigo, H. Effect of Particle Size of Graphites on Electrical Conductivity of Graphite/polymer Composite. *Compos. Interfaces* **1999**, *6*, 483–495.

(24) Barber, A. H.; Cohen, S. R.; Wagner, H. D. Measurement of Carbon Nanotube-Polymer Interfacial Strength. *Appl. Phys. Lett.* **2003**, *82*, 4140–4142.

(25) Tsuda, T.; Ogasawara, T.; Deng, F.; Takeda, N. Direct Measurements of Interfacial Shear Strength of Multi-Walled Carbon nanotube/PEEK Composite Using a Nano-Pullout Method. *Compos. Sci. Technol.* **2011**, *71*, 1295–1300.

(26) Kim, J. Y.; Kim, B. H.; Hwang, J. O.; Jeong, S. J.; Shin, D. O.; Mun, J. H.; Choi, Y. J.; Jin, H. M.; Kim, S. O. Flexible and Transferrable Self-Assembled Nanopatterning on Chemically Modified Graphene. *Adv. Mater.* **2013**, *25*, 1331–1335.

(27) Film, L. G.; Kim, B. H.; Kim, J. Y.; Jeong, S.; Hwang, J. O.; Lee, D. H.; Shin, D. O.; Choi, S.; Kim, S. O. Surface Energy Modification by Spin-Cast, Large-Area Graphene Film for Block Copolymer Lithography. *ACS Nano* **2010**, *4*, 5464–5470.

(28) Kim, J. Y.; Lim, J.; Jin, H. M.; Kim, B. H.; Jeong, S. J.; Choi, D. S.; Li, D. J.; Kim, S. O. 3D Tailored Crumpling of Block-Copolymer Lithography on Chemically Modified Graphene. *Adv. Mater.* **2016**, *28*, 1591–1596.

(29) Jin, H. M.; Park, D. Y.; Jeong, S. J.; Lee, G. Y.; Kim, J. Y.; Mun, J. H.; Cha, S. K.; Lim, J.; Kim, J. S.; Kim, K. H.; et al. Flash Light Millisecond Self-Assembly of High χ Block Copolymers for Wafer-Scale Sub-10 Nm Nanopatterning. *Adv. Mater.* **2017**, *29*, 1–7.

(30) Severin, N.; Rabe, J. P.; Kurth, D. G. Fully Extended Polyelectrolyte-Amphiphile Complexes Adsorbed on Graphite. *J. Am. Chem. Soc.* **2004**, *126*, 3696–3697.

(31) Schlüter, A. D.; Rabe, J. P. Dendronized Polymers: Synthesis, Characterization, Assembly at Interfaces, and Manipulation. *Angew. Chemie - Int. Ed.* **2000**, *39*, 864–883.

(32) Tuinstra, F.; Baer, E. Epitaxial Crystallization of Polyethylene on Graphite. *J. Polym. Sci. Part C Polym. Lett.* **1970**, *8*, 861–865.

(33) Prokhorova, S. A.; Sheiko, S. S.; Mourran, A.; Azumi, R.; Beginn, U.; Zipp, G.; Ahn, C. H.; Holerca, M. N.; Percec, V.; Möller, M. Epitaxial Adsorption of Monodendron-Jacketed Linear Polymers on Highly Oriented Pyrolytic Graphite. *Langmuir* **2000**, *16*, 6862–6867.

(34) Rabe, J. P.; Buchholz, S. Direct Observation of Molecular Structure and Dynamics at the Interface between a Solid Wall and. *Phys. Rev. Lett.* **1991**, *66*, 2096–2099.

(35) Rabe, J. P.; Buchholz, S. Commensurability and Mobility in 2-Dimensional Molecular-Patterns on Graphite. *Science* **1991**, *253*, 424–427.

(36) McClements, J.; Buffone, C.; Shaver, M. P.; Khellil, S.; Koutsos, V. Poly(styrene-Co-Butadiene) Random Copolymer Thin Films and Nanostrucutres on a Mica Surface: Morphology and Contact Angles of Nanodroplets. *Soft Matter* **2017**, *13*, 6152–6166.

(37) Fetters, L. J.; Lohse, D. J.; Milner, S. T.; Graessley, W. W. Packing Length Influence in Linear Polymer Melts on the Entanglement, Critical, and Reptation Molecular Weights. *Macromolecules* **1999**, *32*, 6847–6851.

(38) Fetters, L. J.; Lohse, D. J.; Graessley, W. W. Chain Dimensions and Entanglement Spacings in Dense Macromolecular Systems. *J. Polym. Sci. Part B Polym. Phys.* **1999**, *37*, 1023–1033.

(39) Ying, Q.; Chu, B. Overlap Concentration of Macromolecules in Solution. *Macromolecules* **1987**, *20*, 362–366.

(40) Rubinstein, M.; Colby, R. H. *Polymer Physics*; Oxford University Press: Oxford, 2003.

(41) Nečas, D.; Klapetek, P. Gwyddion: An Open-Source Software for SPM Data Analysis. *Cent. Eur. J. Phys.* **2012**, *10*, 181–188.

(42) Markiewicz, P.; Goh, M. C. Atomic Force Microscopy Probe Tip Visualization and Improvement of Images Using a Simple Deconvolution Procedure. *Langmuir* **1994**, *10*, 5–7.

(43) Fung, S. Y.; Keyes, C.; Duhamel, J.; Chen, P. Concentration Effect on the Aggregation of a Self-Assembling Oligopeptide. *Biophys. J.* **2003**, *85*, 537–548.

(44) Yuan, Y.; Lee, T. R. Contact Angle and Wetting Properties. In *Surface Science Techniques*; Springer: Berlin, 2013; pp 3–34.

(45) Roiter, Y.; Minko, S. AFM Single Molecule Experiments at the Solid-Liquid Interface: In Situ Conformation of Adsorbed Flexible Polyelectrolyte Chains. *J. Am. Chem. Soc.* **2005**, *127*, 15688–15689.

(46) Glynos, E.; Pispas, S.; Koutsos, V. Amphiphilic Diblock Copolymers on Mica: Formation of Flat Polymer Nanoislands and Evolution to Protruding Surface Micelles. *Macromolecules* **2008**, *41*, 4313–4320.

(47) Zhao, W.; Rafailovich, M. H.; Sokolov, J.; Fetters, L. J.; Plano, R.; Sanyal, M. K.; Sinha, S. K.; Sauer, B. B. Wetting Properties of Thin Liquid Polyethylene Propylene Films. *Phys. Rev. Lett.* **1993**, *70*, 1453–1456.

(48) Bal, J. K.; Beuvier, T.; Unni, A. B.; Chavez Panduro, E. A.; Vignaud, G.; Delorme, N.; Chebil, M. S.; Grohens, Y.; Gibaud, A. Stability of Polymer Ultrathin Films (<7 Nm)

Made by a Top-Down Approach. *ACS Nano* **2015**, *9*, 8184–8193.

(49) Macdonald, B. F.; Cole, R. J.; Koutsos, V. The Formation of Dewetting Structures after Evaporation of N-Dodecane on Graphite Studied by Atomic Force Microscopy. *Surf. Sci.* **2004**, *548*, 41–50.

(50) Gan, D.; Cao, W.; Puat, N. E. Thermal Induced Instability of Thin Polymer Films: A Study by Atomic Force Microscopy. *High Perform.Polym.* **2001**, *13*, 259–267.

(51) Rittigstein, P.; Priestley, R. D.; Broadbelt, L. J.; Torkelson, J. M. Model Polymer Nanocomposites Provide an Understanding of Confinement Effects in Real Nanocomposites. *Nat. Mater.* **2007**, *6*, 278–282.

(52) Reiter, G. Dewetting of Highly Elastic Thin Polymer Films. *Phys. Rev. Lett.* **2001**, *87*, 186101–1.

(53) Vilmin, T.; Raphaël, E. Dewetting of Thin Polymer Films. *Eur. Phys. J. E* **2006**, *21*, 161–174.

(54) Keddie, J. L.; Jones, R. A. L.; Cory, R. A. Temperature in Thin Polymer Films. *Faraday Discuss.* **1994**, 219–230.

(55) Yang, H.; Fung, S. Y.; Pritzker, M.; Chen, P. Modification of Hydrophilic and Hydrophobic Surfaced Using an Ionic-Complementary Peptide. *PLoS One* **2007**, *2*, e1325.

(56) Prokhorov, V. V.; Nitta, K. The AFM Observation of Linear Chain and Crystalline Conformations of Ultrahigh Molecular Weight Polyethylene Molecules on Mica and Graphite. *J. Polym. Sci. Part B Polym. Phys.* **2010**, *48*, 766–777.

(57) Takenaka, Y.; Miyaji, H.; Hoshino, A.; Tracz, A.; Jeszka, J. K.; Kucinska, I. Interface Structure of Epitaxial Polyethylene Crystal Grown on HOPG and MoS2 Substrates. *Macromolecules* **2004**, *37*, 9667–9669.

(58) Chen, D.; Handa, H.; Wan, L.; Mao, G. Surface Morphological Evolution of Ultrathin P4VP Films and Generation of Ordered Patterns on Graphite. *Macromol. Rapid Commun.* **2007**, *28*, 1619–1623.

(59) Yang, M.; Koutsos, V.; Zaiser, M. Interactions between Polymers and Carbon Nanotubes: A Molecular Dynamics Study. *J. Phys. Chem. B* **2005**, *109*, 10009–10014.

(60) Glynos, E.; Chremos, A.; Frieberg, B.; Sakellariou, G.; Green, P. F. Wetting of Macromolecules: From Linear Chain to Soft Colloid-like Behavior. *Macromolecules* **2014**, *47*, 1137–1143.

(61) Chremos, A.; Glynos, E.; Koutsos, V.; Camp, P. J. Adsorption and Self-Assembly of Linear Polymers on Surfaces: A Computer Simulation Study. *Soft Matter* **2009**, *5*, 637–645.

(62) Reiter, G. Unstable Thin Polymer Films: Rupture and Dewetting Processes. *Langmuir* **1993**, *9*, 1344–1351.

(63) Reiter, G. Dewetting of Thin Polymer Films. *Phys. Rev. Lett.* **1992**, *68*, 75–78.

(64) Akhrass, S. Al; Vonna, L.; Reiter, G. From Holes to Drop to Toroids: Conditions for the Transcription of Surface Patterns into Three-Dimensional Morphologies via Rim Instabilities in the Course of Dewetting. In *Polymer Surfaces in Motion:*

Unconventional Patterning Methods; Rodríquez-Hernández, J., Drummond, C., Eds.; Springer: Cham, 2015; pp 23–42.

(65) Spangler, L. L.; Torkelson, J. M.; Royal, J. S. Influence of Solvent and Molecular Weight on Thickness and Surface Topography of Spin-Coated Polymer Films. *Polym. Eng. Sci.* **1990**, *30*, 644–653.

(66) Milchev, A. I.; Milchev, A. A. Wetting Behavior of Nanodroplets: The Limits of Young's Rule Validity. *Europhys. Lett.* **2001**, *56*, 695–701.

(67) Evangelopoulos, A. E. A. S.; Glynos, E.; Madani-Grasset, F.; Koutsos, V. Elastic Modulus of a Polymer Nanodroplet: Theory and Experiment. *Langmuir* **2012**, *28*, 4754–4767.

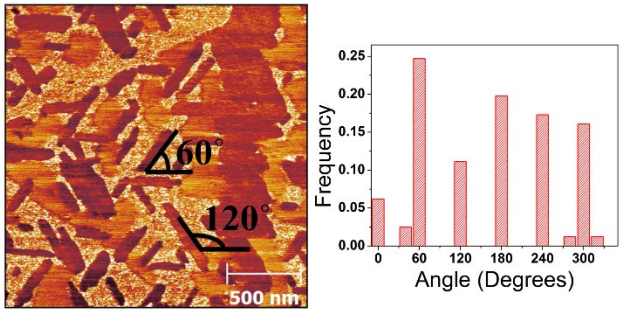

Image for TOC